

# Top quark physics at the LHC with the CMS detector



Sergey Senkin  
School of Physics  
University of Bristol

*A dissertation submitted to the University of Bristol  
in accordance with the requirements of the degree of  
Doctor of Philosophy in the Faculty of Science*

Autumn 2013

# **Declaration**

I declare that the work in this dissertation was carried out in accordance with the Regulations of the University of Bristol. The work is original except where indicated by special reference in the text and no part of the dissertation has been submitted for any other degree. Any views expressed in the dissertation are those of the author and in no way represent those of the University of Bristol. The dissertation has not been presented to any other University for examination either in the United Kingdom or overseas.

Signed: .....

Date: .....

# Contents

<b>1</b>	<b>Introduction</b>	<b>1</b>
<b>2</b>	<b>Theoretical background</b>	<b>2</b>
2.1	Standard Model . . . . .	2
<b>3</b>	<b>The LHC and the CMS detector</b>	<b>3</b>
3.1	The Large Hadron Collider . . . . .	3
3.2	The CMS Detector . . . . .	6
3.2.1	Inner Tracking System . . . . .	8
3.2.2	Electromagnetic Calorimeter . . . . .	11
3.2.3	Hadron Calorimeter . . . . .	15
3.2.4	Superconducting Magnet . . . . .	16
3.2.5	Muon System . . . . .	17
3.2.6	Trigger and Data Acquisition . . . . .	21
3.3	Computing . . . . .	21
3.4	Object Reconstruction . . . . .	21
3.4.1	Electron Reconstruction . . . . .	21
3.4.2	Muon Reconstruction . . . . .	21
3.4.3	Jet Reconstruction . . . . .	21
3.4.4	Missing Transverse Energy . . . . .	21
3.5	Summary . . . . .	21
<b>4</b>	<b>High level trigger development for Top Physics</b>	<b>22</b>
<b>5</b>	<b>Top Quark mass measurement</b>	<b>23</b>
<b>6</b>	<b>Differential cross section measurement</b>	<b>24</b>
6.1	Data and Simulation . . . . .	24
6.2	Event Selection . . . . .	24
6.3	Choice of binning . . . . .	24
6.4	Differential cross section measurement . . . . .	24
6.5	Unfolding . . . . .	24
6.6	Systematic Uncertainties . . . . .	24
6.7	Results . . . . .	24
<b>7</b>	<b>Conclusions</b>	<b>25</b>
<b>References</b>		<b>26</b>

# 1. Introduction

Not really sure what to write here

## **2. Theoretical background**

### **2.1 Standard Model**

Yet to be written...

# 3. The LHC and the CMS detector

## 3.1 The Large Hadron Collider

The LHC [1] is currently the largest and the most powerful particle accelerator ever built. It is installed in the 26.7 km tunnel that was originally constructed for the LEP accelerator in the 1980s. The tunnel lies at a depth of 45 m to 170 m underground between the Jura mountain and the Lake Geneva, being the main part of the CERN accelerator complex.

The machine is designed to accelerate proton beams and provide collisions at a centre of mass energy of  $\sqrt{s} = 14$  TeV. Unlike particle-antiparticle colliders, the LHC requires two rings with opposite magnetic dipole fields in order to maintain and collide two counter-rotating proton beams. Since the tunnel was originally designed for the electron-positron LEP, it has an internal diameter of 3.7 m which is not enough to install two separate independent rings. Therefore, a twin-bore magnet design was adopted [2], which also came as a substantial cost-saving measure.

A schematic view of the LHC accelerator chain is shown on Figure 3.1. In the beginning, the protons are obtained by stripping orbiting electrons from hydrogen atoms. Then they are injected into the linear accelerator LINAC2 to reach the energy of 50 MeV and enter the Proton Synchrotron Booster (PSB). The booster accelerates them to 1.4 GeV and passes the beam to the Proton Synchrotron (PS) where the energy rises to 25 GeV. In the next step, protons enter the Super Proton Synchrotron (SPS) where they are accelerated to 450 GeV. Finally, the

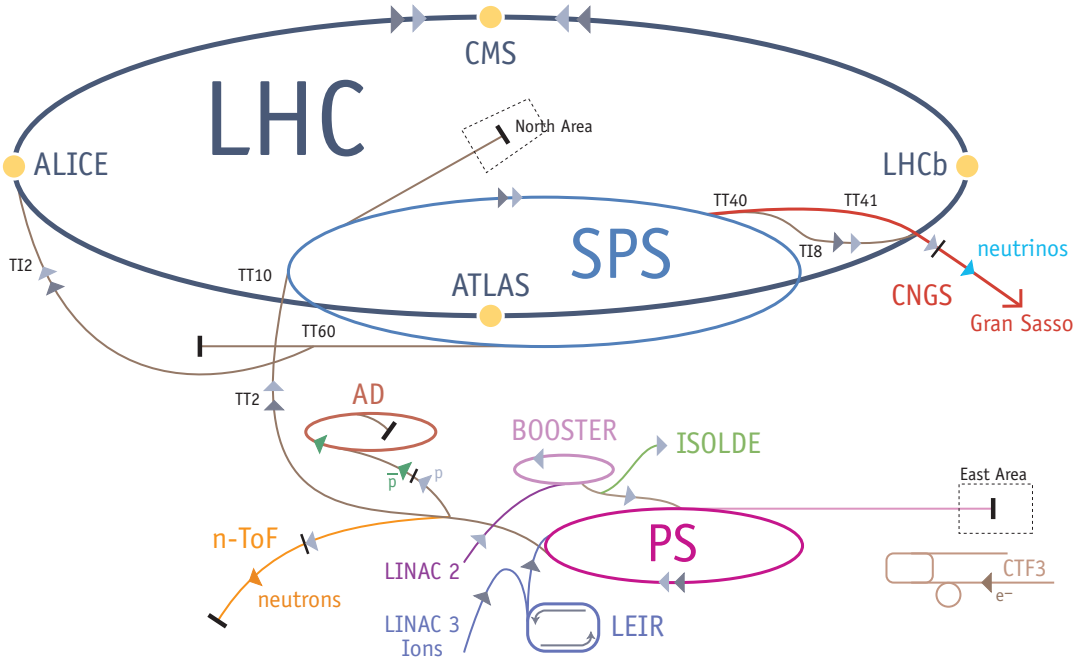


Figure 3.1: CERN accelerator complex.

beam is transferred to the LHC in both clockwise and anti-clockwise directions where it takes about 20 minutes to reach the design 7 TeV energy (per beam).

*[add the number of magnets, total energy stored, number of bunches, bunch spacing etc. ?]*

The LHC has four interaction points, providing collisions to four major experiments. Two of them, CMS and ATLAS, are multi-purpose high-luminosity experiments with a peak luminosity of  $L = 10^{34} \text{ cm}^{-2} \text{ s}^{-1}$ . The other two experiments operate at low luminosities and have more specific physics goals: LHCb studies b-meson decays, and Alice is a dedicated heavy ion experiment.

The instantaneous luminosity of a collider can be calculated as

$$L = \frac{n_1 n_2 f}{4\pi \sigma_x \sigma_y}, \quad (3.1)$$

where  $n_1$  and  $n_2$  are the numbers of particles in each of the colliding bunches,  $f$  is the revolution frequency,  $\sigma_x$  and  $\sigma_y$  are the horizontal and vertical beam sizes, assuming the two beams have the same size.

The number of events generated in the collisions per second is given by

$$N_{events} = L \times \sigma, \quad (3.2)$$

where  $\sigma$  is the cross section of the process under study.

*[add the plots with cross sections and production rates?]*

The LHC started operating on the 10th of September 2008, with the first beams fully circulating in both rings. However, only 9 days later a magnet quench occurred in two sectors of the tunnel, which was caused by an electrical fault due to a bad connection between two magnets. A consequent liquid helium explosion damaged a total of 53 superconducting magnets. Over a year was spent on repairs and tests, and the first collisions were recorded on the 23rd of November 2009 at a centre of mass energy of 0.9 TeV. The following few months showed the continuous ramp up of the beam energies up to 3.5 TeV per beam which was achieved on the 30rd of March 2010 when the LHC physics program started.

Throughout the rest of the 2010 major LHC experiments (CMS and ATLAS) recorded approximately  $40 \text{ pb}^{-1}$  of data, which resulted in the first measurements of various physics processes at the LHC. The following year became the main 7 TeV data-taking period, with about  $5 \text{ fb}^{-1}$  of data recorded by ATLAS and CMS. On the 5th of April 2012 the centre of mass energy was increased to 8 TeV, and July of 2012 marked the first major discovery of a new boson which was later shown to be consistent with the Standard Model Higgs boson, according to

approximately  $21.8 \text{ fb}^{-1}$  of data recorded until early 2013. A long shut-down is planned for the following two years with various upgrades scheduled. The next physics run is expected in 2015 with the beam energy increased up to 6 or 7 TeV.

*[add any upgrade details and distant future plans, like SLHC?]*

## 3.2 The CMS Detector

The Compact Muon Solenoid [3] is a general-purpose detector designed to carry out precise measurements of the Standard Model and the searches for physics beyond it. The primary design requirement was the ability to discover the nature of electroweak symmetry breaking, and the first observation of a Higgs boson was obtained in the Summer of 2012 [4].

The detector is installed at one of the LHC interaction points (Point 5) at about 100 m underground near the French village of Cessy, between the Jura mountains and Lake Geneva. The overall dimensions of the CMS detector are a length of 21.6 m, a diameter of 14.6 m and a total weight of 12 500 t.

The sectional view of CMS is shown on Figure 3.2. In the centre of the detector, tracking and calorimetry systems are surrounded by the superconducting solenoid. On the outermost part of it the magnetic flux is returned through the iron yoke in which the muon system is also integrated. All the sub-systems are discussed in the following sections with more detail.

The cylindrical shape of the CMS detector dictates using the cylindrical coordinate system, with the origin centred at the interaction point, the  $x$ -axis pointing towards the centre of the LHC ring, the  $y$ -axis pointing upwards and the  $z$ -axis pointing along the beamline in the anti-clockwise direction. The azimuthal angle  $\phi$  is measured from the  $x$ -axis in the transverse ( $x - y$ ) plane and the polar angle

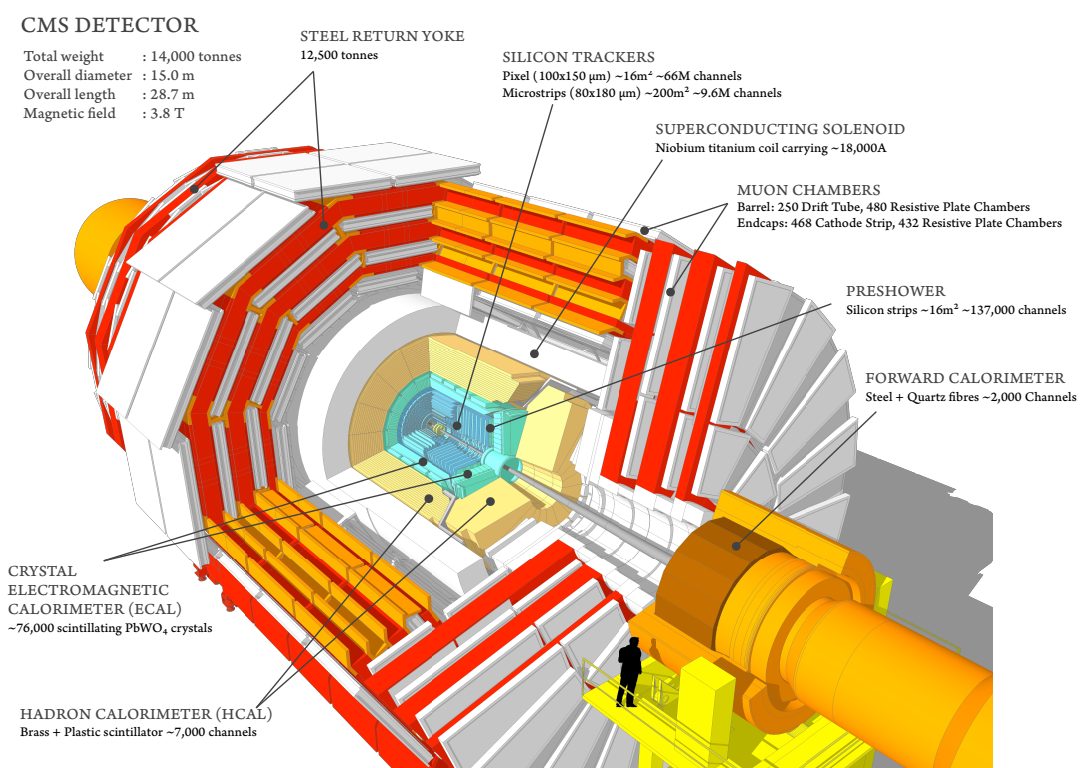


Figure 3.2: Sectional view of the CMS detector.

$\theta$  is measured from the  $z$ -axis. The radial distance to the beamline is denoted as  $r$ . Pseudorapidity is defined as:

$$\eta = -\ln \tan \frac{\theta}{2}. \quad (3.3)$$

This implies that the particles moving in the transverse plane (perpendicular to the beamline) have a pseudorapidity of 0, whereas the beam direction has an infinite pseudorapidity. Considering the cylindrical shape of the detector, it has the barrel and the endcaps regions, with the transition occurring at  $\eta = 1.4$ . The momentum and energy transverse to the beamline are denoted by  $p_T$  and  $E_T$  respectively; the imbalance of the energy measured in the transverse plane, called missing transverse energy, is denoted by  $E_T^{\text{miss}}$ .

### 3.2.1 Inner Tracking System

The tracking system lies in the heart of the CMS detector and is the closest to the interaction point where the particle flux has the highest value. This determines high requirements on the configuration of the system. At design luminosity of  $L = 10^{34} \text{ cm}^{-2} \text{ s}^{-1}$  with the bunch spacing of 25 ns, an average of 1000 particles from about 25 proton-proton interactions (pile-up vertices) is expected to traverse the tracker for each bunch crossing. However, up until the long shutdown the bunch spacing of 50 ns was used, which meant the higher number of protons in each bunch leading to approximately twice as higher number of pile-up vertices. Therefore, in order for the particle tracks to be identified reliably and separately for each bunch crossing, the tracker requires a very fine granularity and fast response parameters. Another complication caused by the intense particle flux is the severe radiation damage, so the tracker has to be highly resilient in

operating in the harsh environment for a reasonable lifetime.

To meet these requirements on granularity, response time and radiation resilience, the tracker design was chosen to be based on silicon detector technology. Although capable to meet such conditions, this technology has a disadvantage of a high power density of on-detector electronics. This implies the necessity of an efficient cooling system. Moreover, a large amount of dense material interacting with the particles leads to the higher multiple scattering, bremsstrahlung, photon conversions and nuclear interactions. Therefore, there are complications in the reconstruction of the tracks, meaning some loss of efficiency and precision. This will be discussed in detail later on in the object reconstruction section.

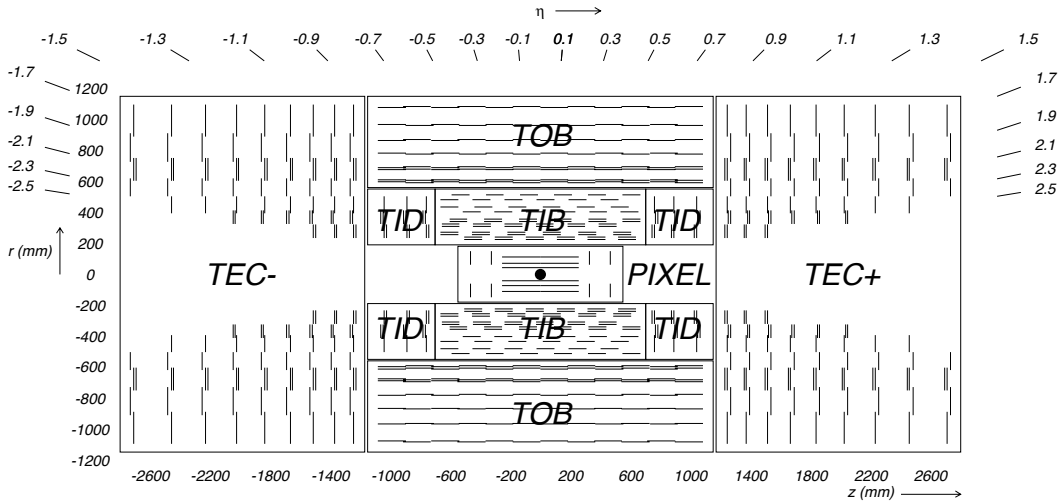


Figure 3.3: Cross-section of the CMS tracker system [3].

Figure 3.3 shows the overall layout of the tracking system. It consists of the inner pixel detector, located in the vicinity of the interaction point, and silicon strip tracker detectors: inner barrel and disks (TIB and TID), outer barrel (TOB) and endcaps (TEC). The geometrical acceptance of the tracker system goes up

to  $|\eta| < 2.5$ . The outer radius of the CMS tracker reaches approximately 110 cm, and its total length is about 540 cm.

The pixel detector consists of three layers of pixel sensors at radii of 4.4 cm, 7.3 cm and 10.2 cm from the beamline in the barrel region. In addition there are two endcap disks on each side at  $|z| = 34.5$  cm and 46.5 cm. The pixel size equals  $100 \times 150 \mu\text{m}^2$  in  $r\phi \times z$  coordinates. The pixel detector has 66 million pixels and the total area of about 1 m<sup>2</sup>.

The silicon strip tracker consists of the several layers of the silicon microstrip detectors. It covers the region between 20 cm to 110 cm in radius and extends up to  $\pm 280$  cm in the z direction. The Tracker Inner Barrel (TIB) is made out of 4 layers and the Tracker Outer Barrel (TOB) has 6 layers in it. The tracker endcaps (TEC) comprise 9 disks, and there are also the tracker inner disks (TID) that consist of 3 discs filling the gap between TIB and TEC. There are 9.3 million silicon strips covering the area of about 200 m<sup>2</sup>. The silicon sensors' thickness varies between 320 and 500  $\mu\text{m}$  and the strip pitch varies from 80  $\mu\text{m}$  in the TIB to 180  $\mu\text{m}$  in TOB and TEC.

The silicon detectors of the tracker, the readout electronics and support structure form a considerable amount of material for the particles traversing from the interaction point. Figure 3.4 [3] shows the material budget of the CMS tracker in units of the radiation lengths<sup>1</sup> ( $X_0$ ). It grows from about 0.4  $X_0$  to 1.8  $X_0$  in the barrel region, and then decreases to about 1  $X_0$  in the endcaps. This causes a substantial conversion rate for photons and electrons in the tracker material; it also will be discussed in more detail in the electron reconstruction section.

---

<sup>1</sup>A material's radiation length is the mean distance over which a high-energy electron loses all but 1/e of its energy by bremsstrahlung; this is equal to 7/9 of the mean free path for pair production by a high-energy photon.

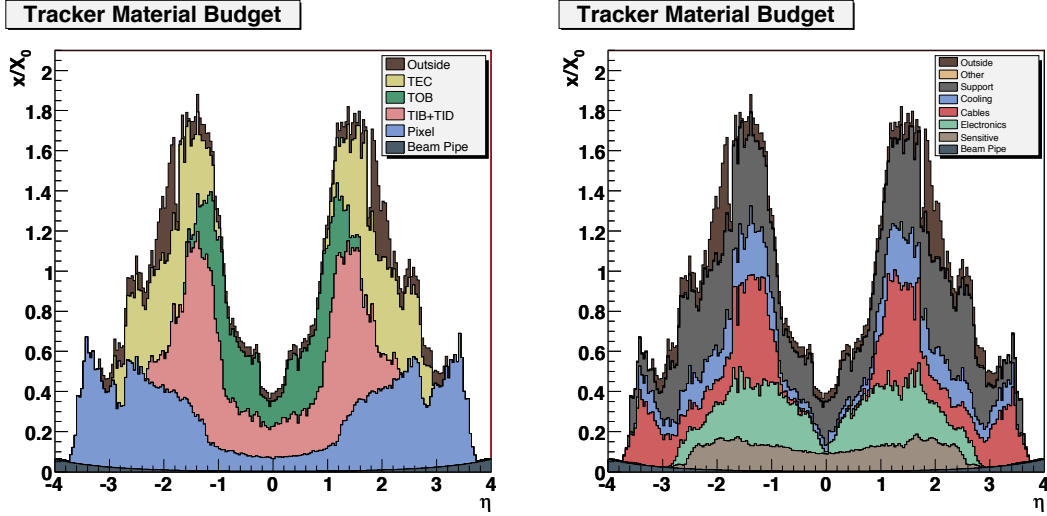


Figure 3.4: Material budget as a function of pseudorapidity  $\eta$  for the different sub-detectors of the tracker (left) and broken down into the functional contributions (right), in units of radiation length [3].

*[perhaps need to add the  $p_T$  resolution plots]*

### 3.2.2 Electromagnetic Calorimeter

The next detector subsystem which is surrounding the tracker is the electromagnetic calorimeter, or ECAL. It is of a primary importance for the analyses described in this thesis, as it provides information for the electron and positron reconstruction. Combination of this information with the one from the tracking system must ensure a precise measurement of electron position and momentum, and also a sufficient background removal. It has to effectively distinguish the energy deposit shape of an electromagnetic particle from the one of a hadronic particle, which requires good segmentation and high resolution.

ECAL is a hermetic, high-granularity, high-resolution scintillating crystal calorimeter consisting of 61 200 lead tungstate ( $\text{PbWO}_4$ ) crystals located in the

central barrel region ( $|\eta| < 1.479$ ), and 7324 crystals in each of the two endcaps ( $1.479 < |\eta| < 3.0$ ). All crystals are followed by photodetectors reading and amplifying their scintillation: avalanche photodiodes (APD) are used in the barrel, and vacuum phototriodes (VPTs) are used in the endcaps. These different choices were caused by the configuration of the magnetic field and the expected level of radiation.

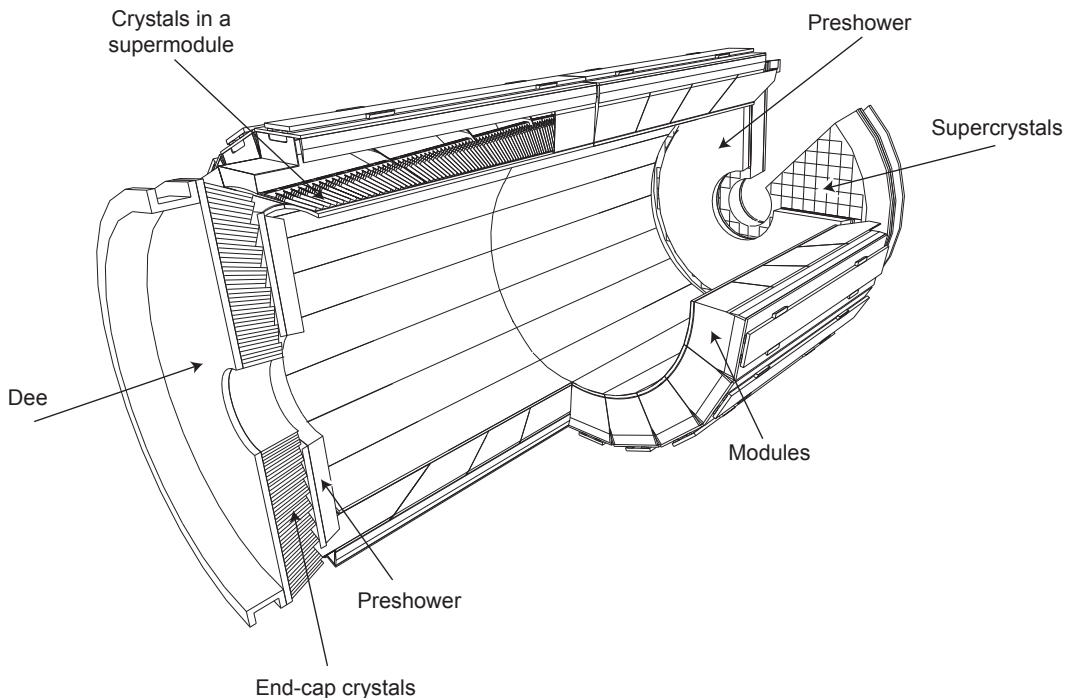


Figure 3.5: Layout of the CMS electromagnetic calorimeter [3].

The layout of the ECAL sub-detector is shown on Figure 3.5. An additional preshower detector is used in the endcap region to lower the required detector depth. Its principal aim is to identify neutral pions in the endcaps, but it also helps to distinguish neutral pions and electrons from minimum ionizing parti-

cles and improves the position determination of electrons and photons with high granularity.

Table 3.1: ECAL crystals characteristics

	Barrel	Endcaps
number of crystals	61 200	14 648
crystal cross-section in $(\eta, \phi)$	$0.0174 \times 0.0174$	varies
crystal cross-section at the front	$22 \times 22 \text{ mm}^2$	$28.62 \times 28.62 \text{ mm}^2$
crystal cross-section at the rear	$26 \times 26 \text{ mm}^2$	$30 \times 30 \text{ mm}^2$
crystal length	$230 \text{ mm (} 25.8X_0 \text{)}$	$220 \text{ mm (} 24.7X_0 \text{)}$

The main geometrical characteristics of the ECAL crystals are shown in Table 3.1. The choice of lead tungstate was driven by the constraints of the CMS design. It is a very dense material ( $8.28 \text{ g/cm}^3$ ) with a short radiation length of  $X_0 = 0.89 \text{ cm}$ , which allows to include the calorimeter inside the compact magnet. Lead tungstate also has a small Molière radius<sup>1</sup> of 2.2 cm, which allows a calorimeter with fine granularity. Finally, the crystals emit 80 % of their scintillation light in just 25 ns, however the light yield is relatively low. At  $18^\circ\text{C}$ , about 4.5 photoelectrons per MeV are collected, which requires a cooling system capable of keeping the crystal temperature stable within  $\pm 0.05^\circ\text{C}$  to preserve energy resolution [5].

The energy-dependent resolution of the calorimeter can be parameterised as follows [3]:

$$\left(\frac{\sigma}{E}\right)^2 = \left(\frac{S}{\sqrt{E}}\right)^2 + \left(\frac{N}{E}\right)^2 + C^2. \quad (3.4)$$

---

<sup>1</sup>The Molière radius  $R_\mu$  is a characteristic constant of a material giving the scale of the transverse dimension of the fully contained electromagnetic showers initiated by an incident high energy electron or photon. It is defined as the radius of a cylinder containing an average of 90 % of the shower's energy deposition.

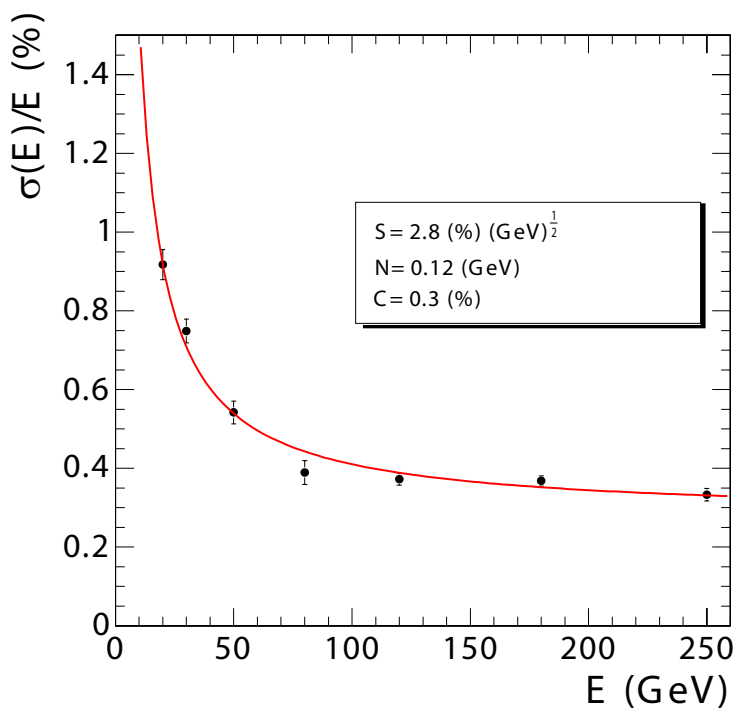


Figure 3.6: ECAL energy resolution derived from the test beam measurements as a function of deposited energy. The stochastic, noise, and constant contributions are shown [3].

where  $S$  is the stochastic term,  $N$  is the noise term, and  $C$  is the constant term. Figure 3.6 shows the energy resolution measured using incident electrons, during the beam tests in 2004.

### 3.2.3 Hadron Calorimeter

The hadron calorimeter (HCAL) is the next sub-detector located mostly inside the solenoid and completing the CMS calorimetry system. It is essential for the measurement of hadron jets and missing transverse energy.

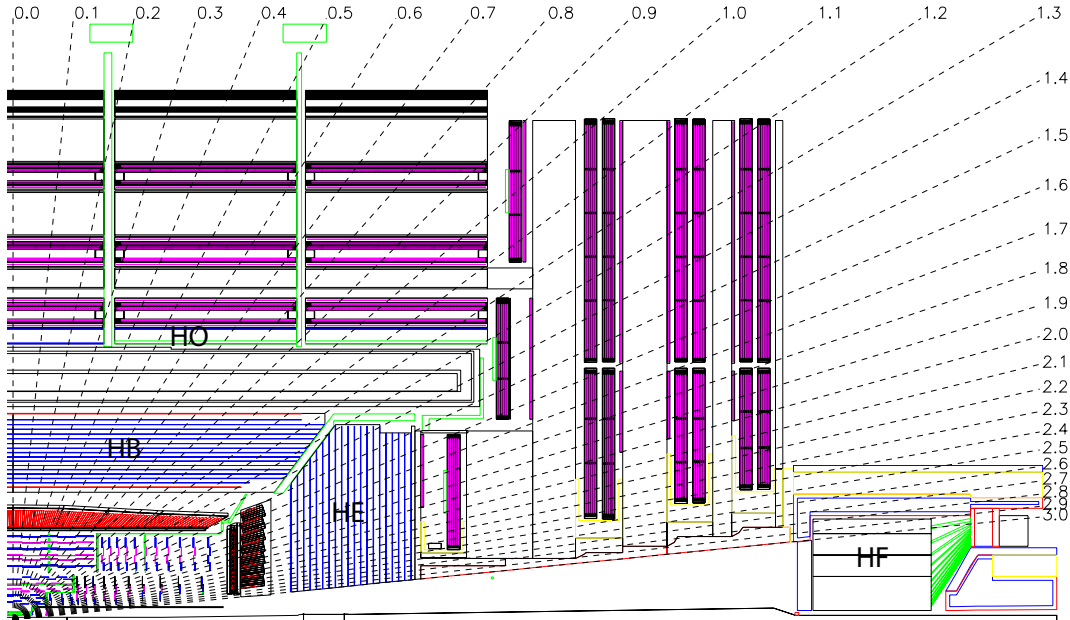


Figure 3.7: Longitudinal view of the CMS detector showing the locations of the hadron barrel (HB), endcap (HE), outer (HO) and forward (HF) calorimeters [3].

As shown on Figure 3.7, HCAL consists of four subsystems: the hadron barrel calorimeter (HB), the hadron endcap calorimeter (HE), the hadron outer calorimeter (HO) and the hadron forward calorimeter (HF). The barrel and endcap parts (HB, HE) cover the pseudorapidity range up to  $|\eta| < 3.0$ , and the for-

ward part (HF) extends it to a total coverage of  $|\eta| < 5.0$ . HCAL surrounds ECAL from its outer limit of 1.77 m from the beamline, to the inner limit of the magnet coil at 2.95 m from the beamline. However, due to space limitations the barrel calorimeters do not contain complete hadronic showers, therefore an outer calorimeter (HO) was designed to measure the energy leakage. It is placed in the muon system just outside of the solenoid in the barrel region.

HCAL is a sampling calorimeter consisting of alternating layers of brass and stainless steel absorbers, and plastic scintillators as active elements. The choice of the absorber material was caused by its large hadronic interaction length and its property of being non-magnetic, which is crucial in the strong magnetic field of the CMS magnet. The scintillation light is guided by embedded wavelength-shifting (WLS) fibres. The light from the WLS is then transmitted via a network of clear fibres, arranged in read-out towers, to hybrid photodiodes (HPDs) [3].

Both HB and HE scintillators have a granularity of  $\Delta\eta \times \Delta\phi = 0.087 \times 0.087$  for  $|\eta| < 1.6$ , and  $\Delta\eta \times \Delta\phi = 0.17 \times 0.17$  for  $|\eta| \geq 1.6$ . The tower segmentation of the forward calorimeter (HF) varies from  $\Delta\eta \times \Delta\phi = 0.175 \times 0.175$  at  $|\eta| = 3.0$  to  $\Delta\eta \times \Delta\phi = 0.3 \times 0.35$  at  $|\eta| = 5.0$ . The HF is placed at about 11 m from the interaction point, and is essential to reconstruct very forward hadron jets. Together with HO, it provides the hermeticity of the calorimetry system, making it possible to measure the transverse missing energy to a reasonable precision.

*[perhaps need to add the energy resolution plots]*

### 3.2.4 Superconducting Magnet

The superconducting solenoid is a very important part of the CMS detector, essentially giving it its name. The magnet has a length of 12.5 m, diameter of

6.3 m and mass of 220 t. Although it was initially designed to sustain a uniform magnetic field of 4 T within the 5.9 m diameter free bore, operation at 3.8 T was chosen in order to increase the lifetime. The magnetic field is returned by a massive iron yoke. The main parameters of the CMS magnet are shown in Table 3.2.

Table 3.2: Parameters of the CMS superconducting solenoid [5] [6].

Field	3.8 T
Inner Bore	5.9 m
Length	12.5 m
Number of Turns	2168
Current	18 160 kA
Stored energy	2.3 GJ

The large bending power of the solenoid is required to bend the high energy particles to an extent where the good momentum resolution is achieved. The design requirement for the strength of the magnetic field was the ability to unambiguously determine the sign of the electric charge for muons with a momentum of  $\approx 1 \text{ TeV}/c$  [5].

The solenoid coil is constructed from four layers of superconducting high-purity niobium-titanium cable co-extruded with pure aluminium, which acts as a thermal stabiliser. The cold mass is cooled down to 4.5 K by liquid helium. If a fast discharge happens (i.e. caused by a magnet quench), about 3 days are necessary to re-cool the coil.

### 3.2.5 Muon System

The last sub-detector placed on the outermost part of CMS is the muon system. Since the muons are the most penetrating particles detectable by CMS, they

have the cleanest signature and play an important role in many physics analyses. Due to their ability to travel through the many layers of the calorimeters, muons are relatively easy to identify and separate from the background.

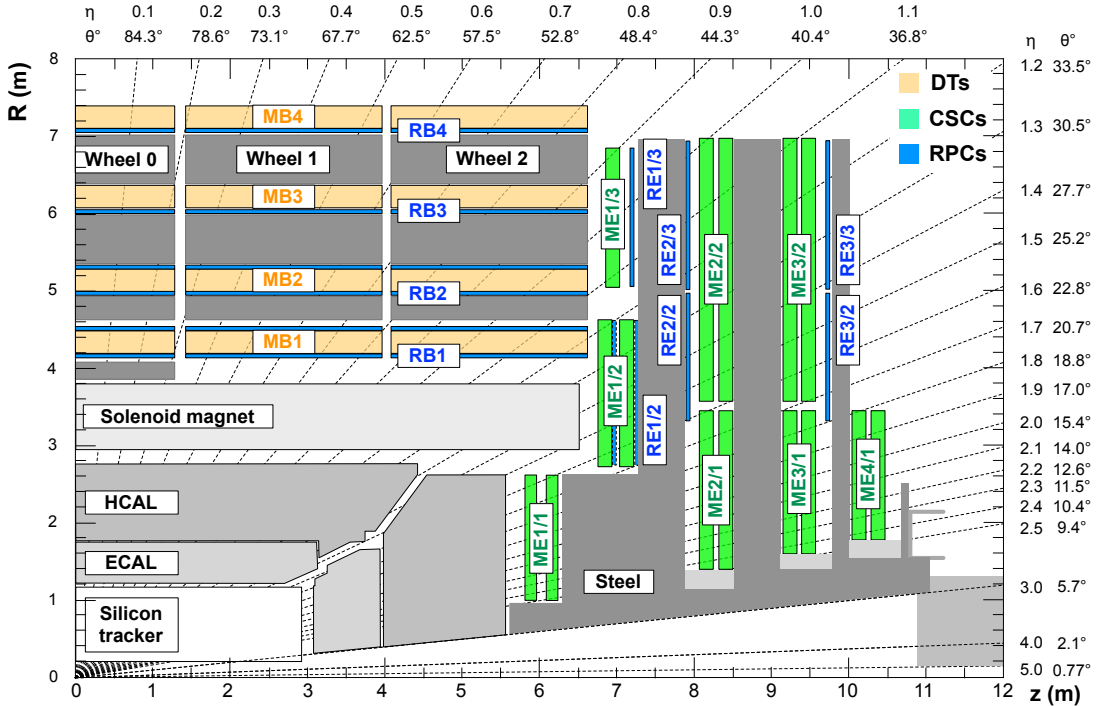


Figure 3.8: Layout of one quarter of the CMS muon system. Four drift tube (DT, in light orange) stations are labeled MB (muon barrel) and the cathode strip chambers (CSC, in green) are labeled ME (muon endcap). Resistive plate chambers (RPC, in blue) are in both the barrel and the endcaps of CMS, where they are labeled RB and RE, respectively.

The layout of the CMS muon system is shown of Figure 3.8. It consists of the drift tubes (DT), cathode strip chambers (CSC) and resistive plate chambers (RPC). The entire system surrounds the solenoid and covers the pseudorapidity region of  $|\eta| < 2.4$ .

The drift tubes are located in the barrel region ( $|\eta| < 1.2$ ). Consisting of four stations, they form concentric cylinders around the beam line; there are 250

drift chambers with about 172 000 sensitive wires in total. When a muon passes through the volume, it knocks electrons off the atoms of the gas, which then follow the electric field and reach the positively-charged wires, providing information on the muon's position. The chambers are filled with the gas mixture of 85 % Ar and 15 % CO<sub>2</sub>, where the muon drift time does not exceed 380 ns. Although this value is bigger than the typical bunch crossing time (25 or 50 ns), it is sufficient because of the small muon rate in this region.

In the endcaps, the cathode strip chambers cover the pseudorapidity region of  $0.9 < |\eta| < 2.4$ . Each of 468 CSCs is a trapezoidal multi-wire proportional chamber consisting of 6 gas gaps with a plane of radial cathode strips and a plane of anode wires which are roughly perpendicular. A charged muon traversing each plane of a chamber causes the gas ionization and a subsequent electron avalanche which produces a charge on the anode wire and an image charge on the cathode strips. The gas used in CSCs is a mixture of Ar, CO<sub>2</sub> and CF<sub>4</sub>.

The resistive plate chambers system is complementary to both DT and CSC systems, and is located in both barrel and endcap regions ( $|\eta| < 2.1$ ). RPCs also operate in avalanche mode with a gas mixture of C<sub>2</sub>H<sub>2</sub>F<sub>4</sub>, C<sub>4</sub>H<sub>10</sub> and SF<sub>6</sub>, and due to an excellent time resolution of about 1 ns they provide fast information for triggering. The spacial resolution is, however, quite limited ( $\approx 1$  cm, compared to  $\approx 100$   $\mu$ m for DTs and CSCs).

The muon momentum is measured in both the tracker and the muon system. As it can be seen on Figure 3.9, both sub-systems contribute to the momentum resolution at different  $p_T$  values. This happens due to the difference in the magnetic field and detector technology. For low- $p_T$  muons, the best momentum resolution is obtained in the tracker, whereas in the high- $p_T$  region the muon

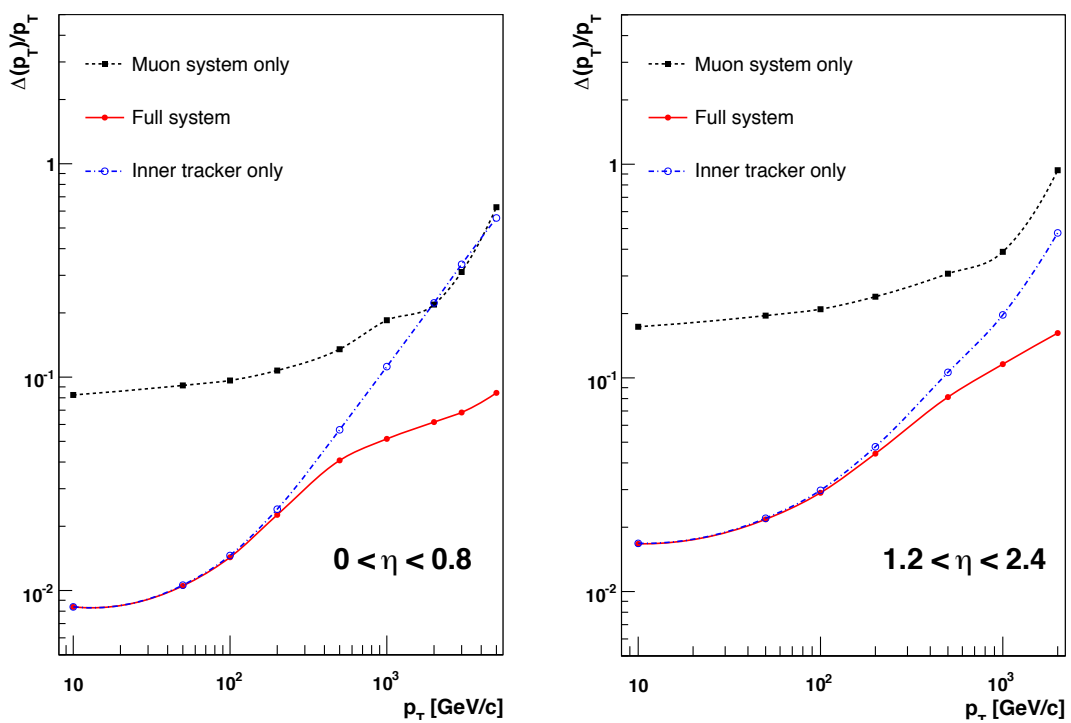


Figure 3.9: The muon transverse momentum resolution as a function of the transverse momentum ( $p_T$ ) using the muon system only (black), the inner tracking only (blue), and both (red), in regions of  $|\eta| < 0.8$  (left) and  $1.2 < |\eta| < 2.4$  (right) [3].

system provides a significant improvement. Therefore, by using information from both the silicon tracker and the muon chambers (i.e. reconstructing the “global muon”), the momentum resolution is improved in the whole  $p_T$  region up to a  $\approx 1$  TeV/c level.

### **3.2.6 Trigger and Data Acquisition**

[1.4 experimental challenge in TDR]

## **3.3 Computing**

## **3.4 Object Reconstruction**

### **3.4.1 Electron Reconstruction**

### **3.4.2 Muon Reconstruction**

### **3.4.3 Jet Reconstruction**

### **3.4.4 Missing Transverse Energy**

## **3.5 Summary**

## **4. High level trigger development for Top Physics**

## 5. Top Quark mass measurement

# **6. Differential cross section measurement**

Measurement of the differential cross section of the top quark pairs with respect to different variables is an important precision measurement, but it can also give hints of new physics. For example, measurement of the missing energy in  $t\bar{t}$  events can represent a search for invisible particles produced in association with top quarks.

## **6.1 Data and Simulation**

## **6.2 Event Selection**

## **6.3 Choice of binning**

## **6.4 Differential cross section measurement**

## **6.5 Unfolding**

## **6.6 Systematic Uncertainties**

## **6.7 Results**

## **7. Conclusions**

# References

- [1] L. Evans and P. Bryant. LHC Machine. *JINST*, 3(08):S08001, 2008. 3
- [2] J.P. Blewett. 200 GeV intersecting storage accelerators. In *Proceedings of The 8th International Conference on High-Energy Accelerators*, page 501, Geneva, Switzerland, 1971. CERN. 3
- [3] The CMS Collaboration. The CMS experiment at the CERN LHC. *JINST*, 3(08):S08004, Aug 2008. 6, 9, 10, 11, 12, 13, 14, 15, 16, 20
- [4] The CMS Collaboration. Observation of a new boson at a mass of 125 GeV with the CMS experiment at the LHC. *Physics Letters B*, 716(1):30–61, 2012. 6
- [5] The CMS Collaboration. *CMS Physics: Technical Design Report Volume 1: Detector Performance and Software*. Technical Design Report CMS. CERN, Geneva, 2006. 13, 17

- [6] CMS Collaboration. Precise mapping of the magnetic field in the CMS barrel yoke using cosmic rays. *Journal of Instrumentation*, 5(03), 2010. 17